Mars 2020 Rover Influence on Wind Measurements at Low Reynolds Number

R. Bardera[1], A. Garcia-Magariño[2], S. Sor[3], M. Urdiales[4]

Instituto Nacional de Técnica Aeroespacial (INTA). Torrejón de Ardoz. Madrid, 28850, Spain,

Mars 2020 rover is the new vehicle dedicated to the Martian surface investigation. This vehicle will transport MEDA, the new meteorological station, including two wind sensors installed in the camera mast. An experimental characterization was conducted to investigate the influence of the Mars 2020 rover in the MEDA wind measurements at low Reynolds numbers. Wind tunnel experiments were conducted using a 1:45th scaled model in a wind tunnel specially designed for these experiments. The velocity was measured using Laser Doppler Anemometry (LDA). A method is proposed in this investigation to calculate a correction factor for the data measurements of wind sensors embarked on rovers dedicated to planetary exploration missions. In particular the method was applied to wind measurements taken by MEDA in the Mars 2020 rover using the LDA measurements and corrections up to 40% in the velocity magnitude and 23º in the deflection angle were found.

I. Introduction

LONG duration planetary surface missions will need to make use of in-situ propulsion. Though most efforts have been focused on the use of the soil chemicals, the wind power recently have shown potential for pushing exploration vehicles on other planets and moons such as Mars, Venus and Titan. The wind energy, used for centuries to power sailing ships, is now being studied to power wind driven craft for

---

planetary exploration. An overview of the wind-driven rovers for planetary exploration can be found in Hajos et al [1], where attention is paid to the new emerging wind-driven science platform concept: the tumbleweed rovers. From a geophysical point of view, increasingly detailed views of Mars of Mariner and Viking studies have revealed the importance of the wind to influence the Martian surface by wind-driven particle mobility [2]. Additionally, the processes of erosion and deposition that have acted on a surface can provide information to know the climatic and environmental conditions that have affected it thought time [3]. Therefore, the actual wind found in the planet or moon to be explored is essential, not only from a geophysical point of view, to gain knowledge on the planet environment and the processed involved in its atmosphere [4-6], but also to design any wind-driven craft.

Previous missions to explore Mars have carried wind sensors to measure the wind velocity and its direction in the Mars surface. The Viking Meteorology Instrument System (VMSI), described in Ref [7], incorporated two wind sensors, based on a hot-film sensor, which were mounted at 90º from each other. Additionally, a quadrant sensor was used to solve the wind direction ambiguity [7-9]. The Mars Pathfinder lander incorporated a meteorology instrument (ASI/MET) to measure, among others, the wind speed and direction at a height of 1.1m. The wind sensor was on the top of a mast and consisted of a composed of six identical hot-wire anemometer elements. Additional details of the wind sensor can be found in Ref [10]. A hot film anemometer for the Martian atmosphere, described by Dominguez et al in Ref [11], as part of the Rover Environmental Monitoring System (REMS), was embarked on the Mars Science Laboratory (MSL) Curiosity rover [11-13]. A new design of the wind REMS sensor is included in the Mars Environmental Dynamic Analyzer (MEDA), which will be hosted by the Mars 2020 rover.

The previous wind sensors have been or will be mounted in rovers, and the wind velocities measured by the sensors are thus affected by the presence of the rover. A method is proposed in this investigation to calculate a correction factor. This method is applied to the case of Mars 2020 rover. A previous study by the authors showed a characterization of the flow field around the Mars 2020 rover at high Reynolds number [14]. During this investigation, the lowest Reynolds number will be addressed.

Due to the low velocities needed in this investigation, where low Reynolds is covered, a wind tunnel is redesign, built and characterized.

II. The Mars 2020 Rover Vehicle

The Mars 2020 rover is a vehicle dedicated to the Martian surface exploration that transports a set of scientific instruments to investigate Mars. The rover is basically composed by a central body with rectangular section supported by six wheels, the vertical mast that supports a remote vision camera and the Mars Environmental Dynamic Analyzer (MEDA) environmental instruments, an articulated robotic arm and the Multi-Mission Radioisotope Thermoelectric Generator (MMRTG) that converts heat from the natural radioactive plutonium in to electrical power for engineering systems and science payload of the rover [15]. MMRTG consist of a cylindrical box connected to heat dissipation fins and two heat exchanger plates [16]. Figure 1 shows a general view of the rover. The wind sensors are indicated as S1 and S2.
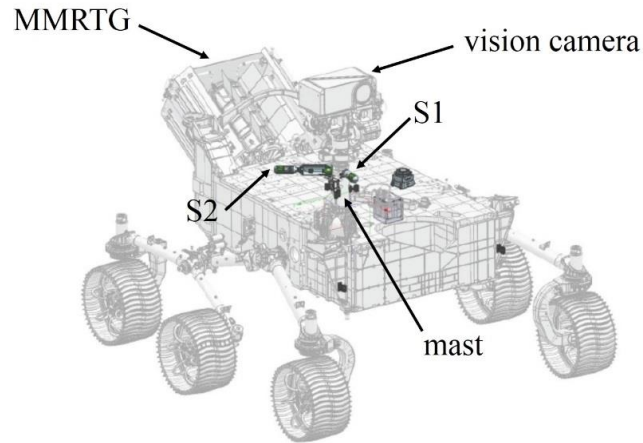

Figure 1. Wind sensors S1 and S2 installed on the Mars 2020 rover

The rover vehicle will be moving on the Mars surface from an initial position R$_o$ to a generic position R* as indicated in Fig. 2. The location of the rover on Mars denoted by $\vec{x}_R$ is given by its position system based on three parameters as follows,

$$\vec{x}_R = f(\varphi, \lambda, R_M) \tag{1}$$

where λ and φ are the martian longitude and lattitude, respectively, and R$_M$ is the radius of Mars.

Figure 2 shows the local horizon axes, centered in the rover position, denoted by R*. East and North are indicated by the X$_h$ and Y$_h$ axes, respectively. The subscript h indicates horizon.
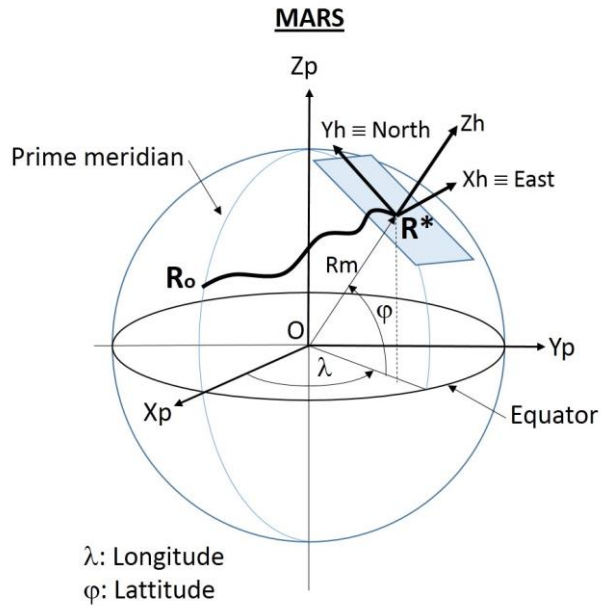
Figure 2. Rover local horizon axes located on Mars

Taking into account the rover is in a static position the majority of time, Fig. 3 shows the rover vehicle when the Mars atmospheric wind V_w is blowing with incidence angle β. A body axes system $O_bX_bY_bZ_b$ fixed to the rover is indicated as well as the body axes in the location of the wind sensor S1. This sensor measures wind velocity distorted by the rover geometry, resulting in a value of velocity magnitude of V_1 and a β_1 angle.
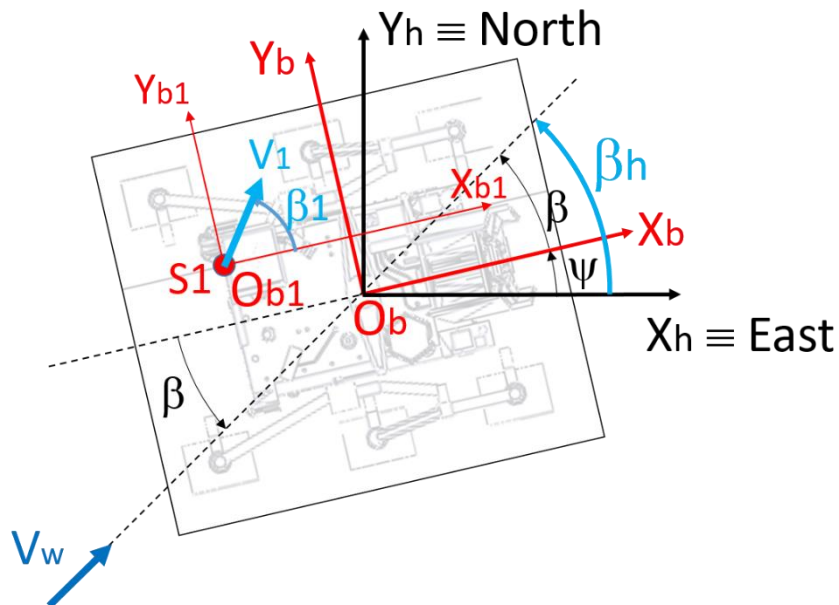

Figure 3. Coordinates systems on the rover vehicle

The location of the rover on the Mars surface will be given by the self-position system, providing the ψ rover yaw angle. Finally, angle $\beta_h = \beta + \psi$, would indicate the wind velocity direction, as follows, $\beta_h = 0$ indicates wind is blowing from West, 90º is coming from South, 180º from East and 270º from North.

III. Wind Velocity Measured by Sensor

Wind velocity measured by the sensor S1 is denoted by vector V_1, forming an angle of attack α_1 and yaw β_l, as indicated in Fig. 4. Since the rover intercepts the flow this velocity is different from the atmospheric wind in both, modulus and direction. Although this study is directed to the sensor S1, analogous equations would be obtained for the second wind sensor S2.
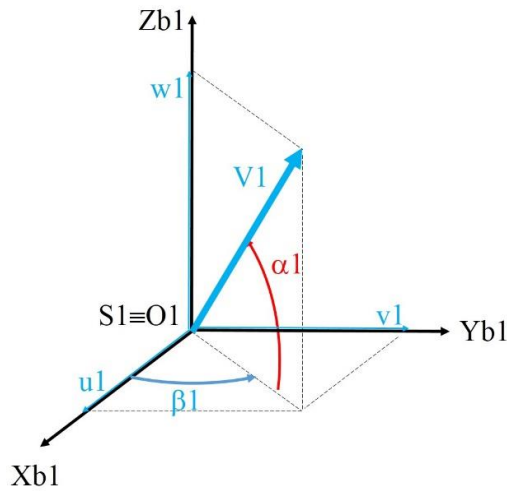

Figure 4. Coordinates body system on the wind sensor S1.

By using a body axes system fixed to the rover and centered in the position of sensor S1, the wind velocity measured by sensor S1 is given as follows,

$$[\vec{V_1}]_b = \begin{bmatrix} u_1 \\ v_1 \\ w_1 \end{bmatrix} = \begin{bmatrix} V_1 \cos\alpha_1 \cos\beta_1 \\ V_1 \cos\alpha_1 \sin\beta_1 \\ V_1 \sin\alpha_1 \end{bmatrix} \tag{2}$$

where u_1, v_1, w_1 are the rectangular components of the vector $\vec{V_1}$ expressed in body axes, and α_l and β_l are the attack and yaw angles, respectively.

On the other hand, the modulus of the perturbed velocity V_1 measured by sensor S_1 is given by,

$$V_1 = \sqrt{u_1^2 + v_1^2 + w_1^2} \tag{3}$$

This velocity can be related with the undisturbed wind velocity V_w by means of the following expression,

5

$$V_1 = V_W \cdot F_1(\beta) \tag{4}$$

where $F_1(\beta)$ is a correction factor that depends on the wind yaw angle, assuming Reynolds number is fixed.

Additional trigonometric relations can be derived as follows,

$$\tan \beta_1 = \left(\frac{v_1}{u_1}\right) \tag{5}$$

$$\sin \alpha_1 = \left(\frac{w_1}{V_1}\right) \tag{6}$$

IV. Determination of Correction Factors by Wind Tunnel Testing

The most appropriated way to determine the correction factors is by wind tunnel testing and by applying the physical similarity laws to the flow over a scaled rover model and full scale Mars rover flow.

Following similarity laws [18], kinematic similarity requires that the model and prototype have the same velocity scale ratio at all points, as follows,

$$\lambda_V = \left(\frac{V_1}{V_W}\right)_{Mars} = \left(\frac{V_1}{U_\infty}\right)_{WT} = F_1 \tag{7}$$

where WT indicates wind tunnel and the kinematic scale results to be equal to the correction factor F_1.

Dynamic similarity exists when the model and prototype have the same length, time and force scale ratios. Dynamic similarity requires flow model and prototype Reynolds numbers must be equal [19] as the flow is incompressible,

$$Re_{Mars} = Re_{WT} \tag{8}$$

On the other hand, flow angles are preserved in geometric similarity, and in this case, flow angle in the position of sensor S1 is given by,

$$\tan \beta_1 = \left(\frac{v_1}{u_1}\right)_{Mars} = \left(\frac{v_1}{u_1}\right)_{WT} \tag{9}$$

A. LDA Measurements

Figure 6 shows the rover model inside the wind tunnel test section when the wind is blowing with yaw angle indicated as β. Laser Doppler Anemometry (LDA) measurements [20] were taken and the LDA axes system is indicated over Fig. 5.
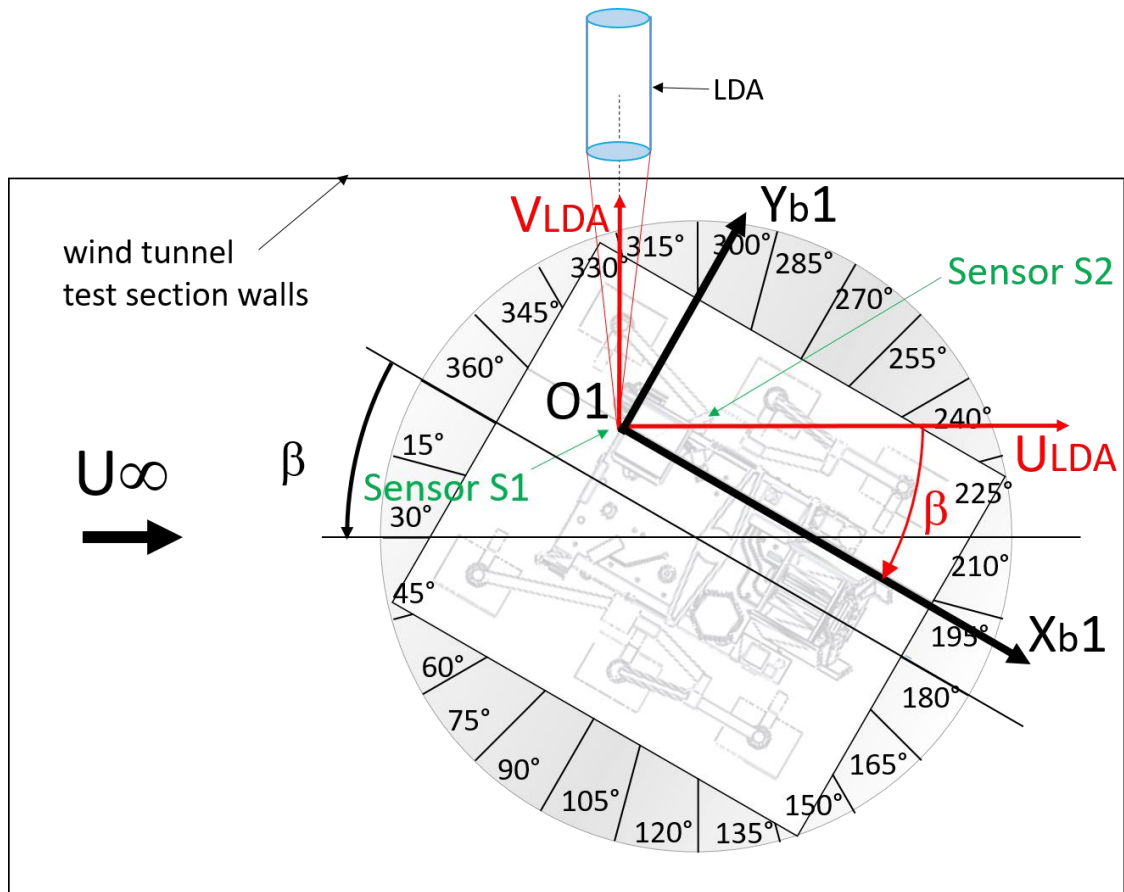
6

Figure 5. Rover model tested in the wind tunnel.

The LDA velocity measured in the sensor S1 position, can be expressed by using a body axes system, as given by the following expression,

$$[\vec{V}_1]_b = \begin{bmatrix} u_1 \\ v_1 \\ w_1 \end{bmatrix} = \begin{bmatrix} u_{LDA} \cos\beta - v_{LDA} \sin\beta \\ u_{LDA} \sin\beta + v_{LDA} \cos\beta \\ w_{LDA} \end{bmatrix} \qquad (10)$$

The modulus of the wind velocity at the location of sensor S1 is,

$$V_1 = \sqrt{u_{LDA}^2 + v_{LDA}^2 + w_{LDA}^2} \qquad (11)$$

The correction factor of the velocity magnitude can be obtained as follows,

$$F_1(\beta) = \frac{V_1}{U_\infty} \qquad (12)$$

where U_∞ is the free stream velocity representing V_W.

7

The angle of the flow at the sensor S1 location is given by a function of the LDA velocity as follows,

$$\tan \beta_1 = \left(\frac{v_1}{u_1}\right) = \frac{\tan\beta + \left(\frac{v_{LDA}}{u_{LDA}}\right)}{1 - \tan\beta \left(\frac{v_{LDA}}{u_{LDA}}\right)} \tag{13}$$

or equivalently,

$$\tan\beta_1 = \tan(\beta + \delta_1) \tag{14}$$

where $\beta_1 = \beta + \delta_1$, and by identifying terms,

$$\tan\delta_1 = \left(\frac{v_{LDA}}{u_{LDA}}\right) \tag{15}$$

where δ_1 corresponds to the deflection of the flow due to the external geometry of the rover vehicle, and this deflection is different for each yaw angle, so that,

$$\delta_1 = f_1(\beta) \tag{16}$$

B. Application to correction of Mars measurements

Correction factors must be expressed as a function of the angle β_1, as this angle is directly determined from rover wind sensor S1 measurements. The velocity correction factor is expressed as follows,

$$F_1(\beta) = \frac{V_1}{V_W} \tag{17}$$

and the deflection angle is given by,

$$\delta1 = g_1(\beta_1) \tag{18}$$

Finally, the free stream velocity and yaw angle will be determined by following expressions,

$$V_W = \frac{V_1}{F_1(\beta)} = V_1 \cdot G_1(\beta_1) \tag{19}$$

where $G_1(\beta_1) = \frac{V_W}{V_1}$.

Functions G_1 and g_1 will be obtained from LDA measurements carried out at the wind tunnel.

$$\beta = \beta_1 - \delta_1 \qquad (20)$$

Figure 6 shows the Mars wind data processing by sensor S1. Additional data would be obtained by sensor S2.
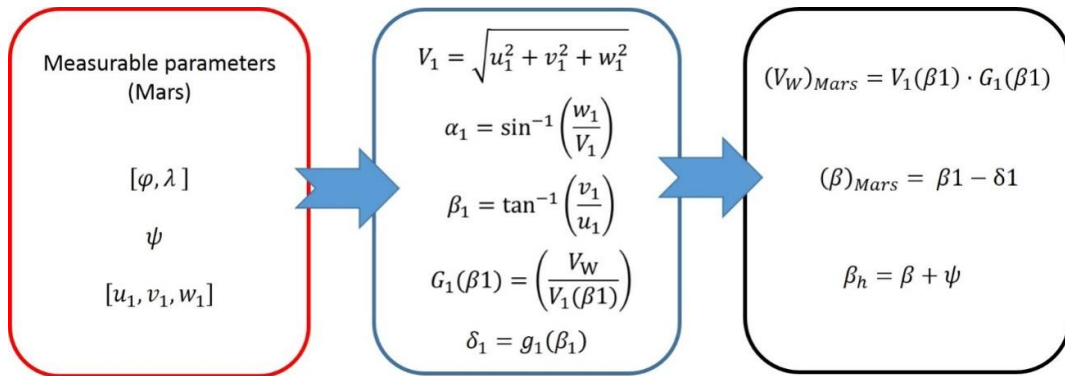

Figure 6. Mars wind data processing by sensor S1

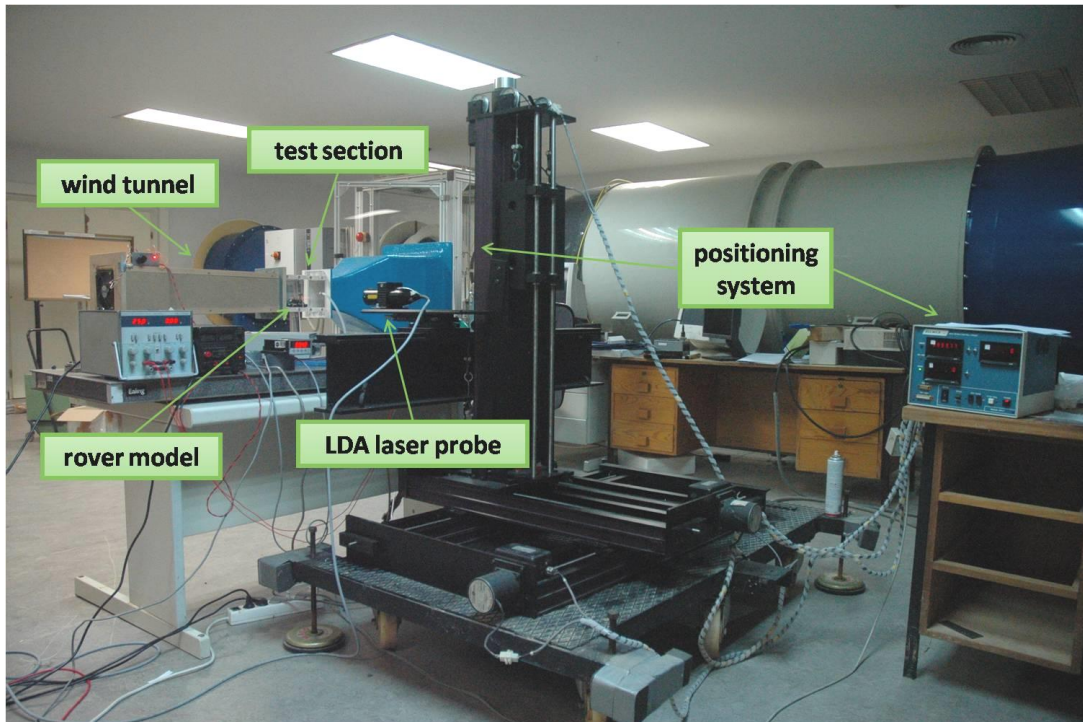## V. Description of the Experimental Facility

Figure 7. Experimental setup

Four modules integrate the experimental facility, namely: the wind tunnel, the LDA system, the positioning system, and the Rover 2020 scaled model. A sketch of the experimental setup can be observed

in Fig. 7. The wind tunnel needed to be designed for this investigation, in order to be adapted to very low Reynolds range.

A. Wind tunnel

In order to obtain the low Reynolds expected in Mars, velocities on the order of 2.5 m/s were required. The wind tunnel used was adapted from a TSI model 8390 to obtain velocities on the order of 2.5 m/s with an acceptable level of turbulence. It is open-looped, and it has a closed test section of square cross section of 100 mm x 100 mm. The total length of the test section is 185 mm, and its walls are made of methacrylate, which allow for a visual access. The air enters through a honeycomb and the contraction ratio is 9:1.

A characterization of the modified wind tunnel was conducted for velocities between 1.8 m/s and 3.5 m/s. The characterization of the tunnel consisted of the determination of the calibration factor, temporal stability, spatial velocity distribution and boundary layer thickness. The calibration factor was obtained (k = 1.0655) showing goodness in the linearity. The temporal stability analysis showed that during 55 second, the root mean square of the velocity was 1.82% of the mean velocity. The velocity distribution in the medium transversal wind tunnel section showed differences of 5% respect to the freestream velocity. The thickness of the boundary layer was measured on the order of 4mm. For further details the meeting paper version may be consulted [21].

B. The LDA System

The LDA used was a commercial system from DANTEC. It consisted of a FlowLite integrated laser-optics unit, a BSA-F60 Flow Processor, the BSA Flow Software and an ultrasonic atomizer to seed the flow. The FlowLite's laser was a continuous 10 mW HeNe laser that has a wavelength of 632.8 nm (red light), with a Gaussian beam diameter of 1.35 mm. The beam separation was 38 mm, and the focal lenses were 400 mm, which led to a fringe distance of 3.35 µm and an ellipsoid measurement volume of 22.6 µm length, 2.13 µm width and 2.14 µm height. The optical frequency shift was 40 MHz, and the velocity span chosen for the tests was 12.5254 m/s. The atomizer generated water droplets with a diameter of the order of five microns, which were small enough to follow the flow.

C. Experimental Setup

The wind sensors in the Mars 2020 rover are located in the two booms that depart from the vertical mast that supports MEDA. One of them is located toward the front part of the rover and has a length of

10

170 mm (sensor S1) and the other is 120º on the right and its length is 400 mm (sensor S2). During the calibration of the wind sensors the influence of the booms has already been considered. This is the reason why the scaled model has no booms. However the influence of the rover has to be studied separately.

A 1:45ᵗʰsubscaled model of the Mars 2020 rover without the booms is used in this investigation. The rover model was built by additive fabrication methods. Figure 8 shows the side and top view of the model in the wind tunnel test section. The typical length of the model is 38 mm and the wind tunnel was running to 2.6 m/s, giving a Reynolds number of Re = 6,770, corresponding to the lowest Reynolds to be expected in atmospheric Mars conditions. A Velmex precision traverse system (see Fig. 7) allowed for the positioning of the LDA laser probe in the three axis directions.
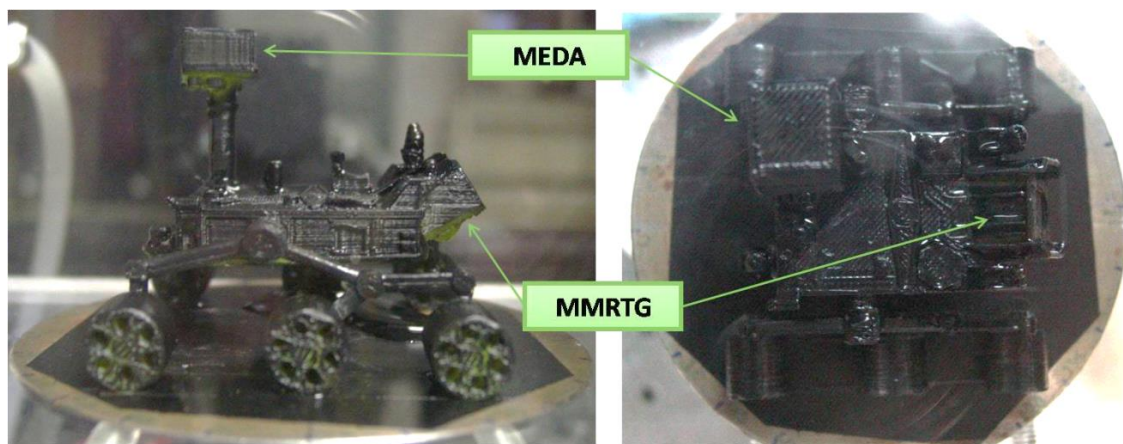

Figure 8. Side view (on the left) and top view (on the right) of the Mars 2020 rover model.

VI. Experimental Results & Discussion

Figure 9 shows the LDA velocity measurements in the location of sensor S1. Plots clearly show a cavity detected in u_{LDA} and v_{LDA} components and located in the range of β from 135º to 240º, that corresponds to the mast wake, where the flow is completely detached, resulting in an invalid region for wind measurement. It is also observed in Fig. 9 that u_{LDA} and v_{LDA} velocity components are of the same order while the w_{LDA} velocity component is small as compared to the others.
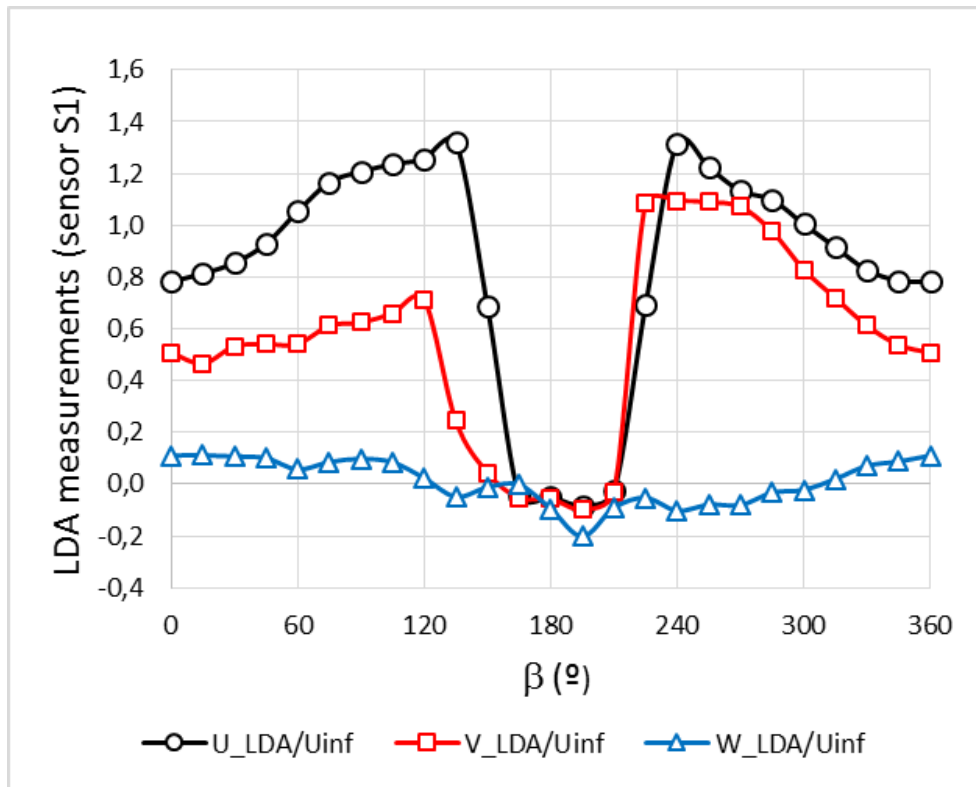
Figure 9. LDA measurements in site of S1

Figure 10 shows the correction factor of the velocity denoted as G_1, represented in two branches separated by the invalid mast wake region. Each valid region was fitted by sixth degree polynomials approximation, with a very high Pearson correlation coefficient denoted by R, as indicated in Fig. 10. Invalid stretch is in the β_1 angle range of 135° and 260°. Factor G_1 indicates that sensor S1 underestimates the velocity up to 40%. %. The expression of the velocity correction factor are the following,

- Range $0° \leq \beta_1 \leq 135°$:

$G_1 = 4E\text{-}11(\beta_1)^6 - 8E\text{-}08(\beta_1)^5 + 6E\text{-}05(\beta_1)^4 - 0.0241(\beta_1)^3 + 5.4516(\beta_1)^2 - 656.92(\beta_1) + 32909$

- Range $260° \leq \beta_1 \leq 348°$:

$G_1 = -2E\text{-}13(\beta_1)^6 - 2E\text{-}11(\beta_1)^5 + 2E\text{-}08(\beta_1)^4 - 2E\text{-}06(\beta_1)^3 - 5E\text{-}05(\beta_1)^2 + 0.0031(\beta_1) + 1.0426$
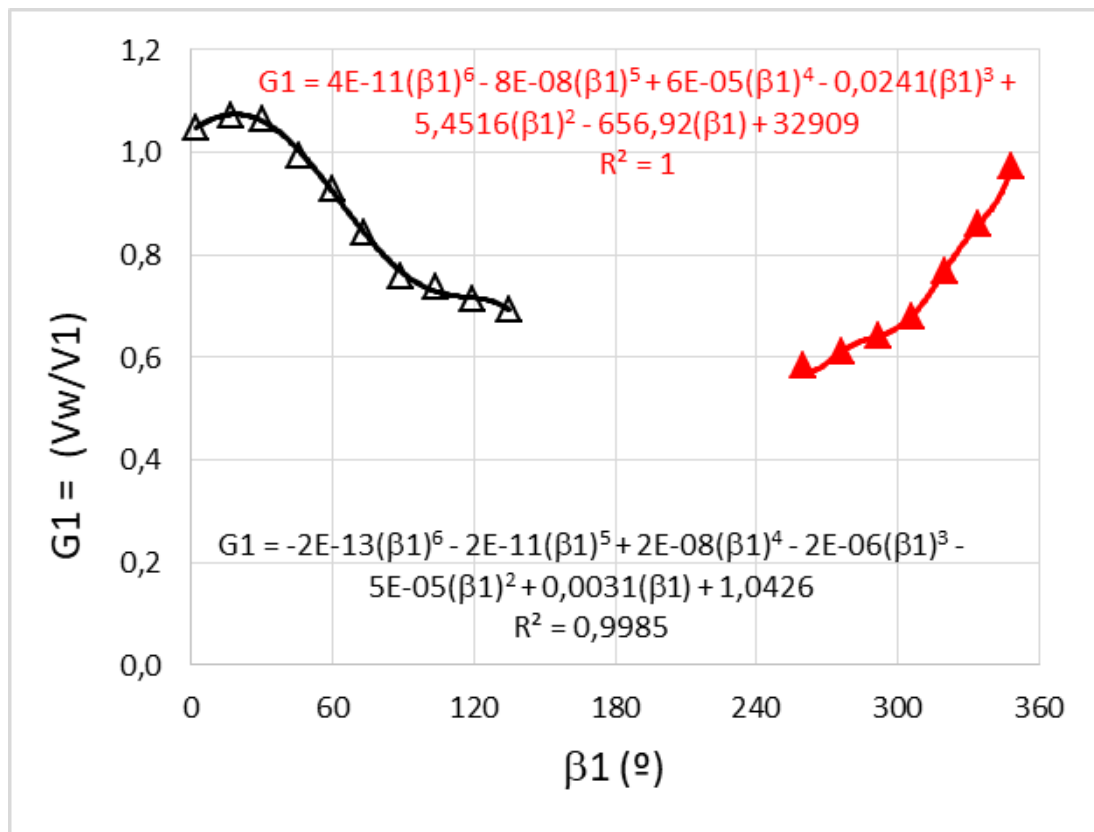
Figure 10. Velocity correction factor for sensor S1.

Figure 11 shows the deflection angle as a function of the β_1 angle and the approximation by a sixth degree polynomial. It is observed that deflection angles up to 22º are found being positive in both branches, given by, for the range $0º \leq \beta_1 \leq 135º$:

$$\delta_1 = 4\text{E-}10(\beta_1)^6 - 8\text{E-}07(\beta_1)^5 + 0.0007(\beta_1)^4 - 0.274(\beta_1)^3 + 64.174(\beta_1)^2 - 7992.6(\beta_1) + 413468$$

while for the range $260º \leq \beta_1 \leq 348º$:

$$\delta_1 = -2\text{E-}11(\beta_1)^6 + 5\text{E-}09(\beta_1)^5 - 1\text{E-}07(\beta_1)^4 - 5\text{E-}05(\beta_1)^3 + 0.0044(\beta_1)^2 - 0.1502(\beta_1) + 17.568$$
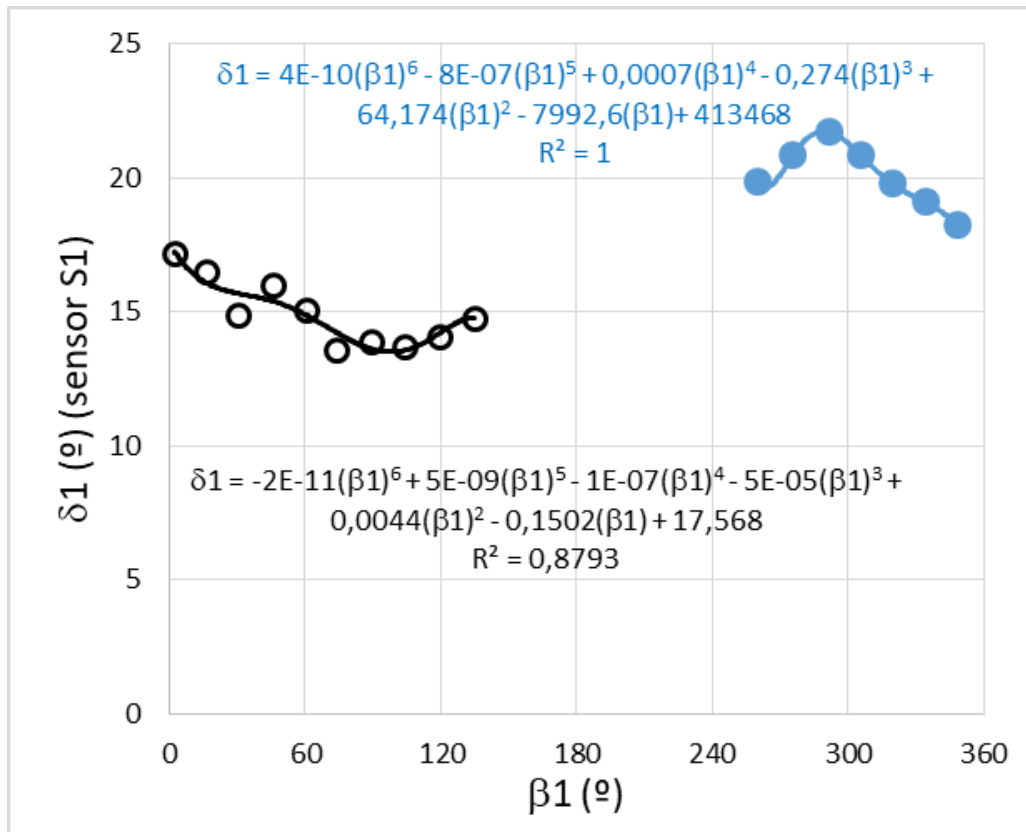
13

Figure 11. Fitting of the deflection angle

Equivalent analysis was performed to the sensor S2. The LDA measurements results are graphed in Fig. 12 showing the cavity, clearly detected over the u_{LDA} component, in the range of β from 30º to 105º, so that corresponds to the mast wake, where the flow is completely detached, resulting in an invalid region for wind measurements from S2. It is observed that both the v_{LDA} and w_{LDA} velocity components are small compared to the u_{LDA} velocity component. This did not occur for sensor S1, however the sensor S2 distance to the mast doubled the sensor S1 distance to the mast, and therefore the influence in sensor S1 is greater.
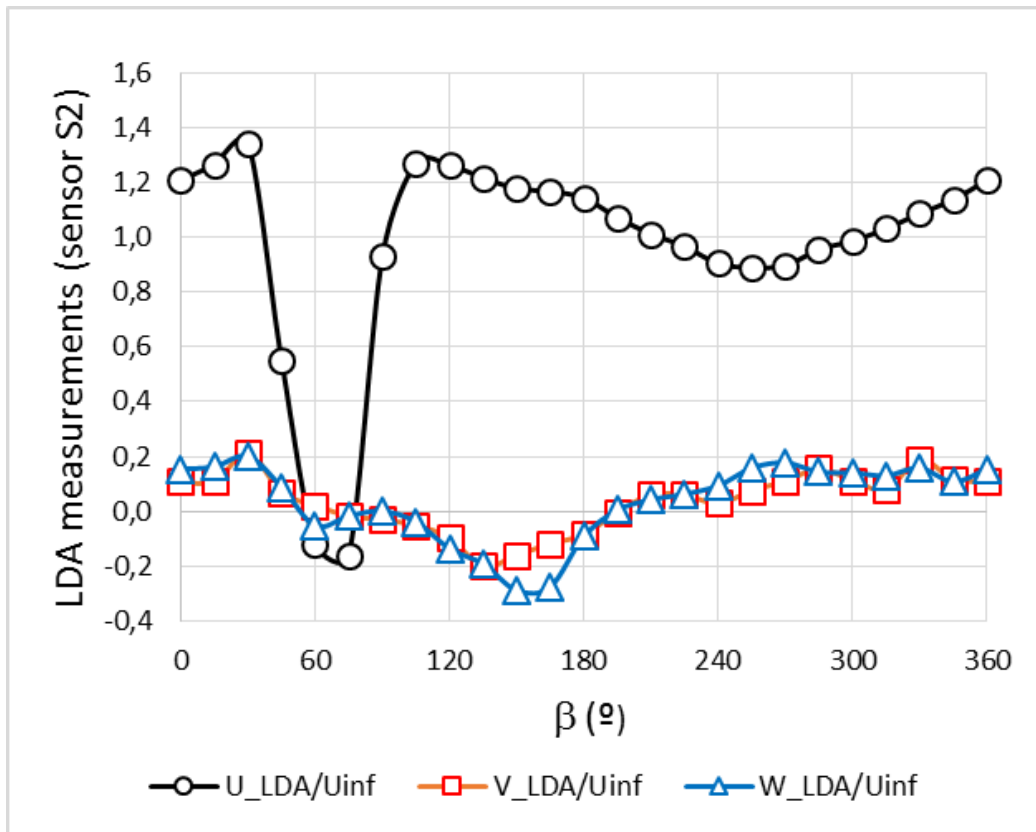
14

Figure 12. LDA measurements in site of S2

Figure 13 shows the correction factor of the velocity G_2 measured by the sensor S2. This factor is represented in two branches separated by the mast wake region. Each valid region was fitted by a parabolic curve and by a sixth degree polynomial approximation, with Pearson correlation coefficients (R) close to the unity, as indicated in the Fig. 13. It is observed that corrections up to 20% are needed and invalid stretch covers the β_2 angle range from 35º to 104º. Expressions in each range are detailed as follows:

- Range $0º \leq \beta_2 \leq 35º$:

$G_2 = -2E\text{-}05(\beta_2)^2 - 0.0022(\beta_2) + 0.8302$

- Range $104º \leq \beta_2 \leq 348º$:

$G_2 = -2E\text{-}14(\beta_2)^6 + 4E\text{-}11(\beta_2)^5 - 3E\text{-}08(\beta_2)^4 + 1E\text{-}05(\beta_2)^3 - 0.0019(\beta_2)^2 + 0.1637(\beta_2) - 4.8027$
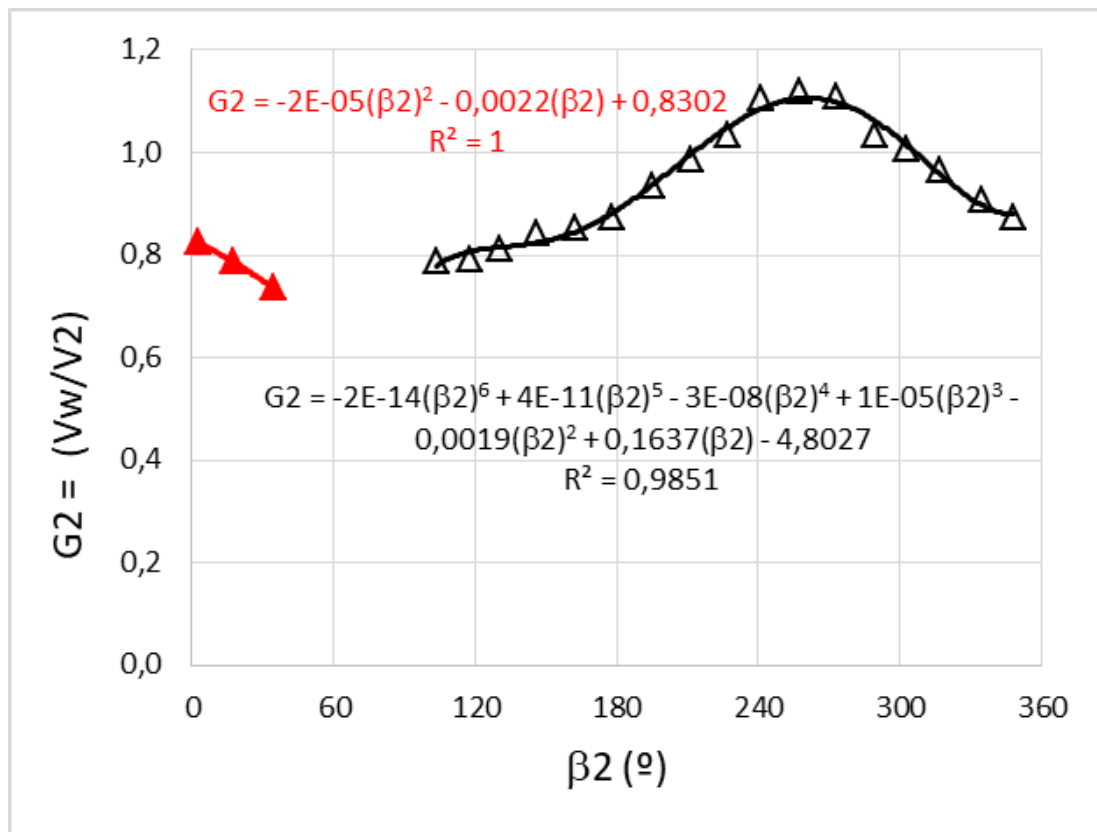
Figure 13. Velocity correction factor for sensor S2

Figure 14 shows the deflection angle as a function of the β_2 angle and the approximation by a sixth degree polynomial. The deflection of the flow in the location of the sensor S2 is below 6º. Expressions in each range are given by:

- Range $0º \leq \beta_2 \leq 35º$:

$$\delta 2 = 0.0041(\beta_2)^2 - 0.092(\beta_2) + 2.7833$$

- Range $104º \leq \beta_2 \leq 348º$:

$$\delta 2 = -7E\text{-}13(\beta_2)^6 + 8E\text{-}10(\beta_2)^5 - 3E\text{-}07(\beta_2)^4 + 2E\text{-}05(\beta_2)^3 + 0.0083(\beta_2)^2 - 1.8012(\beta_2) + 96.053$$
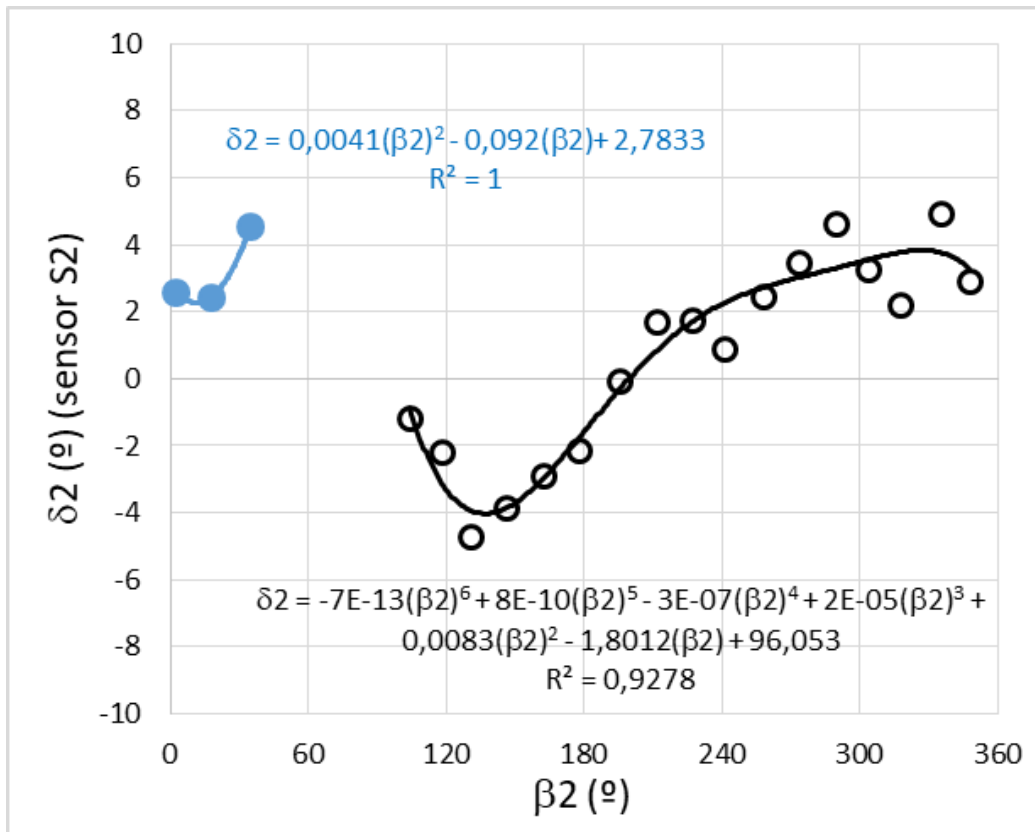
Figure 14. Fitting of the deflection angle for sensor S2.

Finally, the validity of wind measurement ranges for each sensor is graphed in Fig. 15, in a transversal section of the rover mast at medium height. Sensor S1 is valid from 260º (-100º) to 135º and the sensor S2 is valid from 105º to 30º. Whole angular sector is covered by both sensors. Validity regions of these sensors are overlapped in two ranges, the first is from 105 º to 135º and the second one is from 260º to 30º, showing a measurement redundancy. It is observed that validity regions are not symmetric as it would be expected for the wake of mast of cylindrical section, which means that there is an additional effect caused by the whole rover geometry that leads to asymmetry.
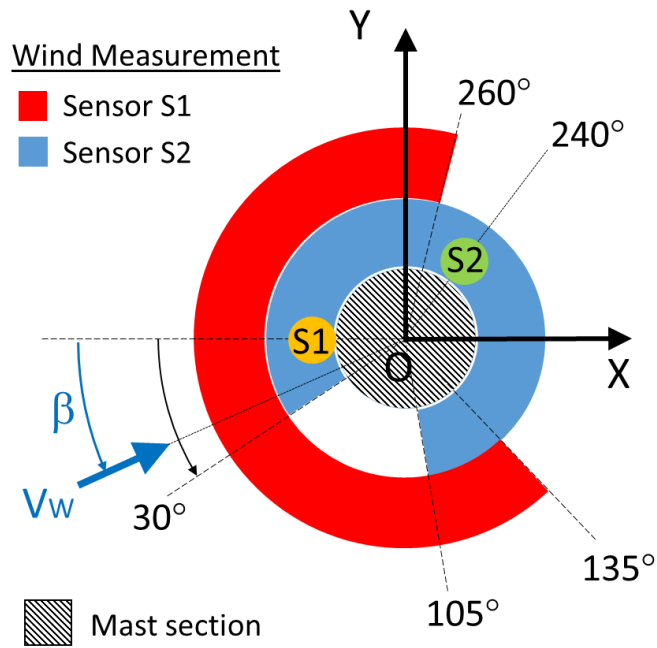
Figure 15. Wind measurement range of each sensor.

VI. Conclusions

The Mars 2020 rover has been developed as a new vehicle to investigate the Martian surface. The new meteorological station MEDA (Mars Environmental Dynamic Analyzer) with atmospheric instruments will be installed on the rover mast, including two wind sensors.

The flow around the wind sensors was investigated by wind tunnel testing a subscale rover model. A specific tunnel in order to be adapted to very low Reynolds range was redesign, built and characterized. Flow measurements were taken using a laser Doppler anemometer (LDA) at different wind incidence angles. Results have demonstrated that the presence of the rover modified the flow as "seen" by the wind sensor. The modified flow, in both, velocity magnitude and direction was studied in order to evaluate the effects of the rover external geometry. Moreover, the corresponding correction factors, in velocity magnitude and direction were determined from experimental results, in order to correct the future data that will be sent by the rover from Mars. It was found, for sensor S1, corrections up to 40% in the velocity magnitude and 23º in the deflection angle, while for sensor S2 corrections were below 20% in velocity magnitude and 6º in the deflection angle. Additionally, the influence of the whole rover geometry turned out to lead to asymmetric validity regions for the sensors.

Acknowledgements

References

[1] Hajos, G. A., Jones, J. A., Behar, A., and Dodd, M., An overview of wind-driven rovers for planetary exploration, 43rd AIAA Aerospace Science Meeting and Exhibit, 10-13 January 2005, Reno, Nevada.

[2] Sullivan, R. et al. Wind –driven particle mobility: Insights from Mars Exploration Rover Observations at "El Dorado" and the surroundings at Gusev Crater. Journal of Geophysical Research 113 (E06S07). 2008. doi:10.1029/2008JE003101.

[3] Golombek, M. P., et al. Erosion rates at the Mars Exploration Rover landing sites and long-term climate on Mars. Journal of Geophysical research 111 (E12S10). 2006. doi:10.1029/2006JE002754.

[4] Petrosyan, A. et al, The Martian Atmospheric Boundary Layer, Reviews of Geophysics, 49, RG-3005/2011. American Geophysics Union.

[5] Leovy, C. B., Martian Meteorology, Ann. Rev. Astron. Astrophys. 1979, 17: 387-413. Annual reviews Inc. 1979.

[6] Colaïtis, A., Spiga, A., Hourdin, F., Rio, C., Forget, F. and Millour, E. A thermal plume for the Martian convective boundary layer. Journal of Geophysical Research: Planets 118, pp 1468-1487, 2013. doi:10.1002/jgre.20104.

[7] Chamberlain, T. E., Atmospheric measurements on Mars: the Viking Meteorology Experiment, Bulletin American Meteorological Society, Vol.: 57, No. 9, pp.:1094-1104, Sept. 1976.

[8] Hess, S. L., Henry, R. M., Kuettner,J., Leovy, C. B., Ryan, J. A., Meteorology Experiments: The Viking Mars Lander, Icarus, 16, pp. 196 -204 (1972). Academic Press,Inc. 1972.

[9] Greene, G. C. et al, Flow-field measurements around a Mars Lander model using hot-film anemometers under simulated Mars surface conditions. Langley Research Center NASA TN D-6820. NASA Washington DC. Sept. 1972.

[10] Seiff, A. et al, The atmosphere structure and meteorology instrument on the Mars Pathfinder Lander, Journal of Geophysical Research, Vol.: 102, No., E2, pp. 4045-4056, Feb. 25, 1997. American Geophysical Union, 1997.

[11] Domínguez, M., Jiménez, V., Ricart, J., Kowalski, L., Torres, J., Navarro, S., Romeral, J., Castañer, L., A hot film anemometer for the Martian atmosphere. Planetary and Space Science. Elsevier, 2008.

[12] Gómez-Elvira and REMS Team, Environmental Monitoring Instrument for Mars Exploration. Lunar and Planetary Science XXXIX (2008).

[13] Gómez-Elvira, J. et al, REMS: The Environmental Sensor Suite for the Mars Science Laboratory Rover. Space Sci. Rev (2012) 170 pp. 583-640.Springer, 2012.

[14] Bardera Mora, R., Sor Mendi S., García-Magariño García, A., Gómez Elvira, J., Marín M., Navarro S., Torres, J., Carretero, S., "Characterization of the flow around the Mars 2020 Rover". 35th AIAA Applied Aerodynamics Conference.5-9 June 2017, Denver, Colorado AIAA 2017-4228.

[15] Environmental Impact Statement for the Mars 2020 Mission. NASA. Washington DC, 20546. June (2014).

[16] Bhandari, P., Anderson K., CFD Analysis for assessing the effect of wind on the thermal control of the Mars Science Laboratory Curiosity Rover. International Conference on Environmental Systems (ICES). AIAA, 2013, Vail, CO.

[17] Lorenz R.D, Sotzen, K.S. Buoyant thermal plumes from planetary landers and rovers: Application to sizing of meteorological masts. Planetary and Space Science 90, pp. 81-89, 2014.

[18] Barlow, J. B., Rae, W. H. Jr.; Pope, A. Low-Speed Wind Tunnel Testing. 3rd Ed.; John Wiley & Sons, Inc. USA 1999.

[19] White, F. "Fluid Mechanics". Fourth Edition. McGraw-Hill Companies, Inc. 2002.

[20] Albrech, H. E. Borys, M., Damaschke, N. and Tropea, C. Laser Doppler and Phase Doppler Measurement Techniques, Springer, New York, NY, USA, 2003.

[21] Bardera, R., Garcia-Magariño, A., Sor, S. and Urdiales, M. "LDA characterization of the Mars 2020 rover influence on the wind measurements at low Reynolds", 2018 Applied Aerodynamics Conference, AIAA AVIATION Forum, (AIAA 2018-2856)